

## The magnetic recoil spectrometer (MRSt) for time-resolved measurements of the neutron spectrum at the National Ignition Facility (NIF)

J. A. Frenje, T. J. Hillsabeck, C. W. Wink, P. Bell, R. Bionta, C. Cerjan, M. Gatu Johnson, J. D. Kilkenny, C. K. Li, F. H. Séguin, and R. D. Petrasso

Citation: [Review of Scientific Instruments](#) **87**, 11D806 (2016); doi: 10.1063/1.4959164

View online: <http://dx.doi.org/10.1063/1.4959164>

View Table of Contents: <http://scitation.aip.org/content/aip/journal/rsi/87/11?ver=pdfcov>

Published by the [AIP Publishing](#)

---

### Articles you may be interested in

[Time-resolved measurements of the hot-electron population in ignition-scale experiments on the National Ignition Facility \(invited\)a](#)

Rev. Sci. Instrum. **85**, 11D501 (2014); 10.1063/1.4890537

[Measurements of fuel and ablator pR in Symmetry-Capsule implosions with the Magnetic Recoil neutron Spectrometer \(MRS\) on the National Ignition Facilitya](#)

Rev. Sci. Instrum. **85**, 11E104 (2014); 10.1063/1.4886418

[The magnetic recoil spectrometer for measurements of the absolute neutron spectrum at OMEGA and the NIF](#)

Rev. Sci. Instrum. **84**, 043506 (2013); 10.1063/1.4796042

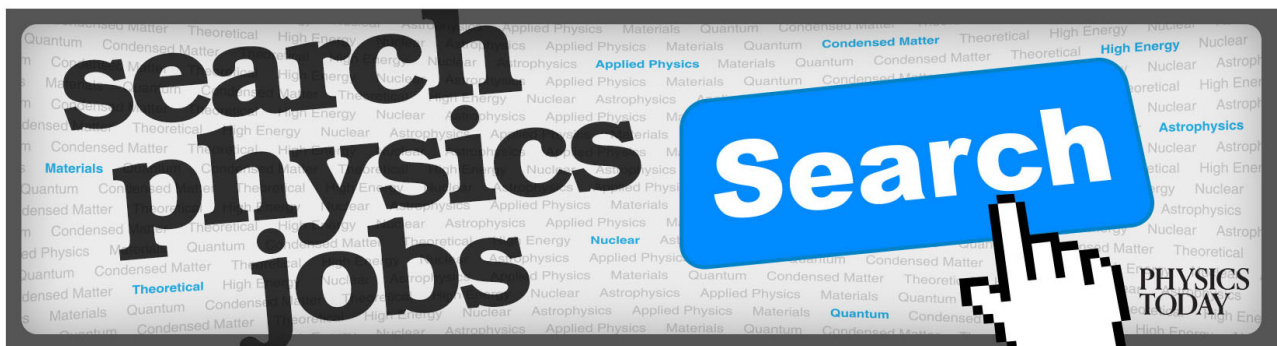
[Measuring the absolute deuterium–tritium neutron yield using the magnetic recoil spectrometer at OMEGA and the NIFa\)](#)

Rev. Sci. Instrum. **83**, 10D912 (2012); 10.1063/1.4738657

[A neutron spectrometer for precise measurements of DT neutrons from 10 to 18 MeV at OMEGA and the National Ignition Facility](#)

Rev. Sci. Instrum. **72**, 854 (2001); 10.1063/1.1323243

---



# The magnetic recoil spectrometer (MRSt) for time-resolved measurements of the neutron spectrum at the National Ignition Facility (NIF)

J. A. Frenje,<sup>1,a)</sup> T. J. Hillsabeck,<sup>2</sup> C. W. Wink,<sup>1</sup> P. Bell,<sup>3</sup> R. Bionta,<sup>3</sup> C. Cerjan,<sup>3</sup>  
 M. Gatu Johnson,<sup>1</sup> J. D. Kilkenny,<sup>2</sup> C. K. Li,<sup>1</sup> F. H. Séguin,<sup>1</sup> and R. D. Petrasso<sup>1</sup>

<sup>1</sup>Massachusetts Institute of Technology, Cambridge, Massachusetts 02139, USA

<sup>2</sup>General Atomics, San Diego, California 92186, USA

<sup>3</sup>Lawrence Livermore National Laboratory, Livermore, California 94550, USA

(Presented 7 June 2016; received 3 June 2016; accepted 23 June 2016;  
 published online 2 August 2016)

The next-generation magnetic recoil spectrometer for time-resolved measurements of the neutron spectrum has been conceptually designed for the National Ignition Facility. This spectrometer, called MRSt, represents a paradigm shift in our thinking about neutron spectrometry for inertial confinement fusion applications, as it will provide simultaneously information about the burn history and time evolution of areal density ( $\rho R$ ), apparent ion temperature ( $T_i$ ), yield ( $Y_n$ ), and macroscopic flows during burn. From this type of data, an assessment of the evolution of the fuel assembly, hotspot, and alpha heating can be made. According to simulations, the MRSt will provide accurate data with a time resolution of  $\sim 20$  ps and energy resolution of  $\sim 100$  keV for total neutron yields above  $\sim 10^{16}$ . At lower yields, the diagnostic will be operated at a higher-efficiency, lower-energy-resolution mode to provide a time resolution of  $\sim 20$  ps. *Published by AIP Publishing.* [<http://dx.doi.org/10.1063/1.4959164>]

## I. INTRODUCTION

Hot-spot ignition planned at the National Ignition Facility (NIF)<sup>1</sup> requires proper assembly of the deuterium-tritium fuel with an areal density ( $\rho R$ ) exceeding  $\sim 1$  g/cm<sup>2</sup> surrounding a  $\sim 5$  keV hot spot with a  $\rho R$  of  $\sim 0.3$  g/cm<sup>2</sup>. Experimental information about the fuel assembly, as manifested by the time evolution of  $\rho R$ , hot-spot ion temperature ( $T_i$ ), and yield ( $Y_n$ ) is therefore critical for understanding the performance of an Inertial Confinement Fusion (ICF) implosion. To date, a set of neutron Time-of-Flight (nTOF) spectrometers<sup>2-4</sup> and a Magnetic Recoil Spectrometer (MRS)<sup>5-8</sup> have been used routinely at the NIF for measurements of the time-integrated neutron spectrum, from which burn-averaged values of  $\rho R$ ,  $Y_n$ , and apparent  $T_i$  have been determined.<sup>9</sup> Although these data have been essential to understand and improve the ignition experiments at the NIF,<sup>10,11</sup> the current diagnostic suite does not provide any detailed information about the time evolution of the fuel assembly, core ion temperature, nuclear burn, and alpha heating. In addition, current x-ray diagnostics, which will progressively deteriorate with increasing yields, provide information about temporal core emission but this information is restricted to the electron temperature and density and not to the fuel assembly. In the context of optimizing the stagnation conditions, the effect of the Residual Kinetic Energy (*RKE*) is also an outstanding issue that needs to be addressed.<sup>12</sup> Simply stated, if the *RKE* of the fuel and ablator during assembly is not effectively transferred to hot-spot thermal

energy, the ignition-relevant conditions will not be achieved. By monitoring the time evolution of  $\rho R$  and  $T_i$ , *RKE* can be quantified. As discussed herein, this information can be obtained simultaneously with the next-generation MRS for time-resolved measurements of the ICF neutron spectrum. This new spectrometer, designated below as the MRSt, represents a paradigm shift in our thinking about neutron spectrometers for ICF applications, as it will open a new diagnostic window to NIF implosions.

This paper is structured as follows: Section II discusses how the relative timing and time evolution of  $\rho R$ ,  $T_i$ , and  $Y_n$ , determined from the time-resolved neutron spectrum, can be used to assess the evolution of the fuel assembly, formation of hot spot, and alpha heating. Section III describes the principle and conceptual design of the MRSt. Section IV elaborates on the first simulations of the MRSt performance, and Section V discusses the path forward.

## II. $\rho R(t)$ , $Y_n(t)$ , AND APPARENT $T_i(t)$ FROM THE TIME-RESOLVED NEUTRON SPECTRUM

As discussed extensively in the literature, information about  $Y_n$  and apparent  $T_i$  is obtained from the primary-neutron spectrum, while  $\rho R$  is inferred from the yield ratio between down-scattered and primary neutrons.<sup>2,3,7-9</sup> Thus, a time-resolved neutron spectrum will provide information about  $\rho R(t)$ ,  $Y_n(t)$ , and apparent  $T_i(t)$ . An illustration of the evolution and dependencies of these parameters is made in Fig. 1 for shot N130927. Fig. 1(a) shows simulated  $\rho R(t)$ ,  $Y_n(t)$ , and thermal  $T_i(t)$  when no alpha heating is included in the simulation; Fig. 1(b) shows the same implosion parameters when the alpha heating has been artificially enhanced 4 $\times$  relative to the experimentally inferred value; and Fig. 1(c) shows the same implosion parameters when the alpha heating

Note: Contributed paper, published as part of the Proceedings of the 21st Topical Conference on High-Temperature Plasma Diagnostics, Madison, Wisconsin, USA, June 2016.

<sup>a)</sup>Author to whom correspondence should be addressed. Electronic mail: [jfrenje@psfc.mit.edu](mailto:jfrenje@psfc.mit.edu).

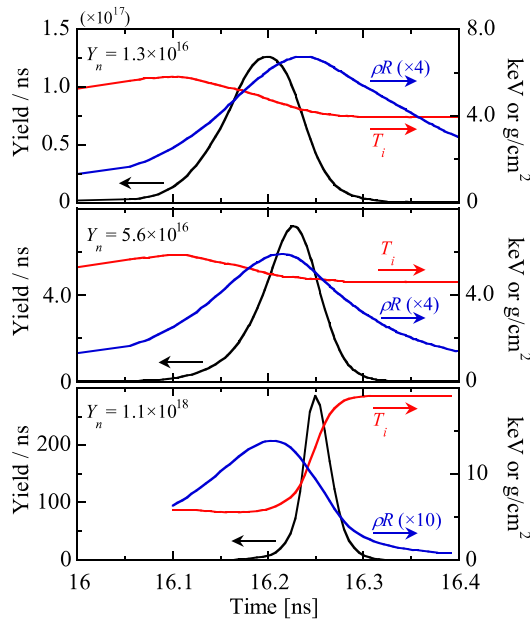


FIG. 1. Post-shot simulations of  $\rho R(t)$ ,  $Y_n(t)$ , and  $T_i(t)$  for shot N130927 with (a) no alpha heating included in the simulation, (b) with alpha heating artificially enhanced 4 $\times$  relative to the experimentally inferred value, and (c) with alpha heating artificially enhanced 83 $\times$ , which is enough heating for the implosion to ignite. As discussed in detail in the text, the relative timing and evolution of these implosion parameters change with changing level of alpha heating.

has been artificially enhanced 83 $\times$ , which is enough for the implosion to ignite. The simulated total yield is indicated in the top-left corner in each figure. As shown by Figs. 1(a)–1(c), the peak burn (or bang time) is progressively getting delayed relative to the timing of peak compression as alpha heating is enhanced. As a result, bang time occurs before and after peak compression in the no-alpha-heating implosion and the ignited implosion, respectively. It is also notable that  $T_i$  decreases and increases during burn in the non-ignited implosions and the ignited implosion, respectively. The opposite is true for the evolution of  $\rho R$ , i.e., it increases in the no-alpha-heating implosion while it decreases in the ignited implosion during burn. In the ignited case,  $\rho R$  is simply decreasing during burn because it is already disassembling due to the increasing internal pressure caused by the run-away reaction and increased  $T_i$ . The burn duration is also getting substantially narrower with increasing alpha heating. These characteristic signatures clearly indicate the importance of an MRSt measurement of the evolution and relative timing of these quantities. As already mentioned, the level of the RKE during burn, which is difficult if not impossible to measure with other diagnostics, can also be probed with the MRSt. Furthermore, MRSt will complement the Advanced Radiographic Capability (ARC)<sup>13</sup> leading to a much deeper understanding of the fuel assembly, hot-spot formation, and stagnation. Additionally, two orthogonal MRSt lines-of-sight would quantify asymmetries in the evolution of the fuel assembly and hot-spot formation and put stringent constraints on the implosion modeling. Folding this type of data with time-resolved core electron temperature measurements would also provide additional insights about the evolution of velocity gradients in the burning core.

### III. MRSt PRINCIPLE AND DESIGN

The experience gained by implementing and using the MRS on OMEGA and the NIF has provided essential input to the design of the MRSt. The guidelines for optimizing the MRS, discussed in Refs. 5–7, have been used and taken to the next level when designing the MRSt. As schematically shown in Fig. 2, the design consists of (1) a thin and small CH<sub>2</sub> (or CD<sub>2</sub>) foil positioned very close to the implosion (most likely attached to the outside of the hohlraum at the equator). The foil has to be positioned close to the implosion to minimize the time spread of different-energy neutrons (at the foil), which generate recoil protons (or deuterons) with one energy; (2) an aperture positioned 600 cm from the foil for selection of forward-scattered recoil protons (or deuterons); (3) two dipoles, positioned just outside the NIF target chamber, with variable and opposing B-field directions that do not introduce any significant time spread of same-energy recoil protons (or deuterons) at the focal plane of the spectrometer. This characteristic is essential to the design, as it minimizes the path-length difference for same-energy particles and thus reduces the time dispersion to a minimum, dictated by the characteristics of the foil and ion-optical aberrations of the dipole system (see Fig. 2 for detailed information about the design); (4) and an ultra-fast pulse-dilation drift tube<sup>14</sup> for detection of the recoil protons (or deuterons) over an energy range of 12–16 MeV (or 10.7–14.2 MeV), which corresponds to a neutron-energy range of 12–16 MeV. The front end of the pulse-dilation

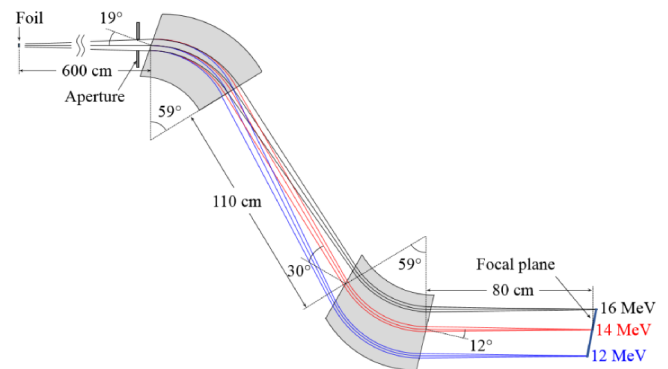


FIG. 2. Conceptual design of the MRSt for the NIF (to scale). This design is based on first-order ion-optical calculations and covers a proton energy range of 12–16 MeV (or 10.7–14.2 MeV deuterons). The aperture in front of the first dipole is positioned 600 cm from a disposable 0.5-mm diameter foil, which is attached to the outside of the NIF hohlraum. For focusing in the dispersive plane and some focusing in the non-dispersive plane, the inclination angle of the incoming protons (or deuterons) is 19° relative to the pole-surface normal. These ions are subsequently bent about 59°, and transported 110 cm to the second dipole with an opposing B-field direction where they are bent once again about 59°. The ions leave the second dipole with an exit angle of about 12° relative to the pole-surface normal. The focal-plane distance is about 80 cm from the exit surface of the second dipole. The length of the focal plane is 23 cm. The signal arrival time for 12–16 MeV protons is 159–187 ns, while it is 238–279 ns for 10.7–14.2 MeV deuterons. The B-field in both dipoles is 1.19 T at the proton central trajectory. For deuterons, the B-field at the central trajectory is 1.58 T. Each dipole also has a magnetic field index of 0.4 for improved focusing characteristics and for minimized path-length differences through the system. Knowing both the geometry and ion-optics of the MRSt allows for a ps-accurate determination and correction of the relative timing of signal particles with different energies.

drift tube will be made of a 23-cm-long,  $\sim 2$ -cm-wide and 1000-Å-thick Cesium-Iodide (CsI) photocathode, positioned at the focal plane of the spectrometer, for production of secondary electrons that are subsequently accelerated by a spatially and time-varying electrical field that aligns and stretches the signal, while drifting about  $\sim 1$  m, before being detected by an array of segmented anodes connected to a multi-channel digitizer. In high-resolution mode, this design provides an energy resolution of  $\sim 100$  keV and a time resolution of  $\sim 20$  ps, as discussed in Sec. IV.

#### IV. SIMULATED MRSt PERFORMANCE

A Monte-Carlo based ion-optical code was developed and used to characterize and optimize the conceptual design of the MRSt when operating in different configurations at the NIF. The results, in terms of energy resolution ( $\Delta E$ ), time resolution ( $\Delta t$ ) and detection efficiency ( $\varepsilon$ ), from that modeling are shown in Table I for the primary-neutron measurements. The different configurations involve different foil thicknesses and aperture areas.

As shown by Table I,  $\Delta t$  is not significantly increased as the aperture area is increased. This is due to the fact that  $\Delta t$  is not primarily driven by the path-length differences through the system, but rather by the focusing properties of the spectrometer, where same-energy recoil protons (or deuterons) emitted from an extended source (the foil) cannot be focused to one point at the focal plane. What the design does is to de-magnify the foil diameter about three times in the dispersive plane, which corresponds to  $\sim 0.1$  mm, or  $\sim 2$  keV (the dispersion is  $\sim 20$  keV/mm) and  $\sim 13$  ps.

Examples of simulated MRSt proton data at the CsI photocathode are shown in Fig. 3 for the three implosions illustrated in Fig. 1. In these simulations, the MRSt was operated in configuration #1 shown in Table I. In the case of the non-ignited implosions (Figs. 3(a) and 3(b)), the down-scattered signal totally dominates the primary signal in the energy range of 12-13 MeV. When the implosion ignites, a narrower energy range must be used for the down-scattered signal measurement.

As alpha heating varies, the timing and evolution of the proton signal from primary neutrons vary relative to the timing and evolution of the signal from down-scattered neutrons. It is also notable that the spectral width of the primary signal

TABLE I. Energy resolution ( $\Delta E$ ), time resolution ( $\Delta t$ ), and detection efficiency ( $\varepsilon$ ) for three different MRSt configurations at the NIF. In these calculations, a 0.5-mm diameter CH<sub>2</sub> (or CD<sub>2</sub>) foil is attached to the outside of the hohlraum at the equator at a distance of 0.3 cm from the capsule. The aperture is positioned 600 cm from the foil. The values in the parentheses are for the CD<sub>2</sub> foil.

Configuration	#1	#2	#3
Foil thickness ( $\mu\text{m}$ )	20 (10)	40 (20)	80 (40)
Aperture area ( $\text{cm}^2$ )	$2 \times 2$	$4 \times 4$	$8 \times 4$
$\Delta E$ (keV)	100 (90)	150 (140)	290 (280)
$\Delta t$ (ps)	13 (25)	13 (25)	15 (27)
$\varepsilon$ ( $\times 10^{-12}$ )	0.72 (0.78)	5.72 (6.20)	22.8 (24.8)

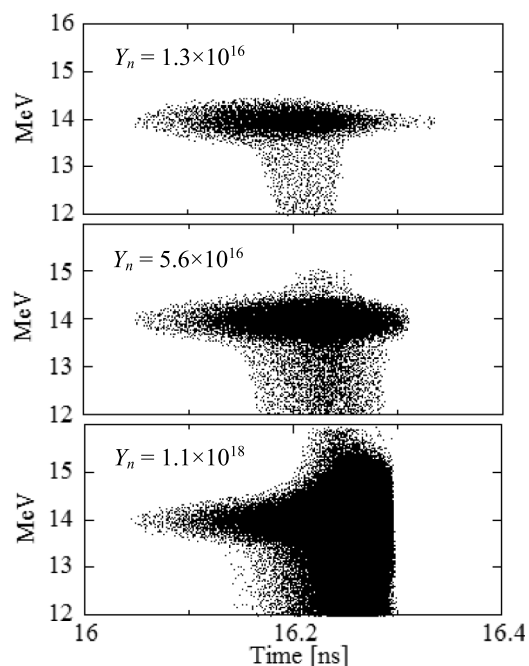


FIG. 3. Simulated MRSt proton data at the CsI photocathode for the three implosions illustrated in Fig. 1. The different flight path times of the different protons has been corrected for in the data. In these simulations, the MRSt was operated in high-resolution mode, i.e., configuration #1 (Table I), generating about 9500, 41 200, and 790 000 signal protons at the CsI photocathode for the three implosions. According to Wink *et al.*,<sup>15</sup> each proton generates  $\sim 1$  secondary electron in the CsI photocathode. See text for additional details.

increases dramatically over a time period of  $\sim 40$  ps, as alpha heating and ion temperature increase, a variation that the MRSt can in principle diagnose. In addition, slicing the MRSt data in time, a determination of  $\rho R(t)$ ,  $Y_n(t)$ , apparent  $T_i(t)$ , and  $RKE(t)$  can be made. Projecting the data onto the energy axis provides the time-integrated spectrum, which is the analogue to the MRS spectrum routinely measured today at the NIF. The burn history is either obtained by projecting the signal onto the time axis for improved statistics or by slicing the data in energy.

As discussed by Hilsabeck *et al.*,<sup>14</sup> the plan is to use a  $\sim 1$ -m-long pulse-dilation drift tube, connected to a 1000-Å-thick CsI photocathode covering the focal plane, to record the MRSt signal. The details of how the MRSt data will be recorded are still being defined. Additionally, an understanding of the pulse-dilation-drift-tube response to the signal protons (or deuterons in case of a CD<sub>2</sub> foil) and background, mainly consisting of neutrons and  $\gamma$ -rays, is discussed by Wink *et al.*,<sup>15</sup> who also discuss the signal-to-background (S/B) required for successful implementation of the MRSt on the NIF.

#### V. SUMMARY AND PATH FORWARD

The accomplished work to date has defined the first-order ion-optical design of the MRSt and its key components on the NIF. This system will provide simultaneous information about the burn history and time evolution of  $\rho R$ , apparent



$T_i$ ,  $Y_n$ , and macroscopic flows during burn, from which an assessment of the evolution of the fuel assembly, hotspot, and alpha heating can be made. According to simulations, the MRSt configuration #1 will provide accurate data with a time resolution of  $\sim 20$  ps and energy resolution of  $\sim 100$  keV for total neutron yields above  $\sim 10^{16}$ . At lower yields, the diagnostic will be operated at a higher-efficiency, lower-energy-resolution mode (configuration #2 or #3) to provide a time resolution of  $\sim 20$  ps.

The next step is to characterize and correct for the higher-order ion-optical aberrations. The optimal size of the pole gap will also be defined. Experiments at the NIF will be undertaken to test the idea of attaching the foil to the outside of the NIF hohlraum at the equator. A determination of the required shielding will be made to meet the required S/B for both the primary and down-scattered neutron measurements. The CsI photocathode response to ions with varying energy will also be measured. In particular, the number of secondary electrons per incoming proton (or deuteron) at a given energy will be determined.

## ACKNOWLEDGMENTS

This work was performed under the auspices of the U.S. Department of Energy by Lawrence Livermore National Laboratory under Contract No. DE-AC52-07NA27344.

- <sup>1</sup>G. H. Miller *et al.*, *Nucl. Fusion* **44**, S228 (2004).
- <sup>2</sup>R. Hatarik *et al.*, *J. Appl. Phys.* **118**, 184502 (2015).
- <sup>3</sup>M. G. Johnson *et al.*, *Rev. Sci. Instrum.* **83**, 10D308 (2012).
- <sup>4</sup>T. Clancy *et al.*, *Proc. SPIE* **9211**, 92110A (2014).
- <sup>5</sup>J. A. Frenje *et al.*, *Rev. Sci. Instrum.* **72**, 854 (2001).
- <sup>6</sup>J. A. Frenje *et al.*, *Rev. Sci. Instrum.* **79**, 10E502 (2008).
- <sup>7</sup>J. A. Frenje *et al.*, *Phys. Plasmas* **17**, 056311 (2010).
- <sup>8</sup>D. T. Casey *et al.*, *Rev. Sci. Instrum.* **84**, 043506 (2013).
- <sup>9</sup>J. A. Frenje *et al.*, *Nucl. Fusion* **53**, 043014 (2013).
- <sup>10</sup>D. T. Casey *et al.*, *Phys. Rev. Lett.* **115**, 105001 (2015).
- <sup>11</sup>T. Ma *et al.*, *Phys. Rev. Lett.* **114**, 145004 (2015).
- <sup>12</sup>A. L. Kritcher *et al.*, *Phys. Plasmas* **21**, 042708 (2014).
- <sup>13</sup>D. Nicola *et al.*, *Proc. SPIE* **9345**, 93450I (2015).
- <sup>14</sup>T. J. Hillsabeck *et al.*, "A stretch/compress scheme for a high temporal resolution detector for the magnetic recoil spectrometer time (MRSt)," *Rev. Sci. Instrum.* (these proceedings).
- <sup>15</sup>C. W. Wink *et al.*, "Signal and background considerations for the MRSt on the National Ignition Facility (NIF)," *Rev. Sci. Instrum.* (these proceedings).